



DFT and Electrochemical Study of Novel Green Corrosion Inhibitor (Pyrantrin) for 1100-H14 Aluminum Corrosion Remediation in 1 M H₂SO₄ Acidic Environment

Benedict U. Ugi^{1*} 

¹ Department of Pure & Industrial Chemistry, University of Calabar, P. M. B. 1115, Calabar – Nigeria.

Abstract: The study on Corrosion Inhibition of 1100-H14 Aluminum in H₂SO₄ Acidic Deploying pyrantrin as a Green Inhibitor was investigated by adopting different experimental methods, including weight loss, electrochemical impedance spectroscopic, potentiodynamic polarization, and computational methods. It was observed that pyrantrin was a good inhibitor for the 1100–H14–type aluminum. Inhibition efficiency was recorded between 42.5 % and 95.2 % for aluminum at 500 ppm and 1500 ppm concentrations. This high inhibition efficiency was attributed to the strong adsorption of the molecules on both metal surfaces. Electrochemical impedance showed higher and increasing charge transfer resistance values and decreasing values for the double-layer capacitance, indicating better inhibition. From quantum calculations, the EHOMO value was higher than that of the ELUMO, while the energy gap was calculated to be 1.9 with a binding energy of 132.9, indicating stronger adsorption and inhibition.

Keywords: Pyrantrin, EIS, adsorption, Langmuir, S275JR mild steel, simulation.

Submitted: January 14, 2023. **Accepted:** August 31, 2023.

Cite this: Ugi BU. DFT and Electrochemical Study of Novel Green Corrosion Inhibitor (Pyrantrin) for 1100-H14 Aluminum Corrosion Remediation in 1 M H₂SO₄ Acidic Environment. JOTCSA. 2024;11(1):253-60.

DOI: <https://doi.org/10.18596/jotcsa.1234194>

***Corresponding author's E-mail:** ugibenedict@gmail.com

1. INTRODUCTION

Like death and taxes, corrosion is something we hope to avoid, but ultimately, it is something we must learn to deal with. Metals, especially aluminum, are widely used in today's world, especially in the fields of engineering – shipping, building, construction, machining, automobile, petroleum, mining, etc. (1-2). The beauty and strength experienced by these metals while in use allow for their wider application. However, the wide application of metal is truncated by the damage caused by the effects of corrosion. This aggressiveness from corrosion could tamper with the metal's durability, tensile strength, malleability, ductility, conductivity, lustrousness, etc. Corrosion, the deterioration of metal under unfavorable environmental conditions, has come a long way and seems only to be managed as hopes of complete eradication of the effects are dripping off, considering the different growing environmental conditions experienced today, especially from greenhouse effects (1,3). The cause of corrosion is widely attributed to the chemistry involved – electrochemical or chemical corrosion process and the processes involved in the preparation and

treatment of these metals before their application, for instance, during acid pickling, acidization, descaling, fracking processes, etc. (2-4). In the corrosion process, two reactions take place. In one, the anodic reaction, metal atoms are ionized and pass into solution, leaving their electrons within the original metal surface (1-3). In the second, the cathodic reaction, the free electrons within the metal are taken up by chemical species such as O₂ and H₂O in reduction reactions. Corrosion inhibitors have been found to be effective and flexible means of corrosion mitigation. Most organic/inorganic compounds containing elements of groups V B and VI B or functional groups of the amine, carbonyl, and alcoholic groups are more effective corrosion inhibitors (2,3-5). The inhibitor is adsorbed on the entire metal surface, preventing the metal's attack. pyrantrin (Figure 1) is used particularly as the embonate [4,4'-methylenebis(3-hydroxy-2-naphthoate)] salt and as an anthelmintic that is effective against intestinal nematodes, including threadworms, roundworms, and hookworms. This study investigates pyrantrin application as an alternative green corrosion inhibitor of 1100-H14 aluminum alloy in a 1 M H₂SO₄ acid environment.

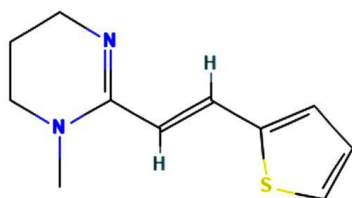


Figure 1: Structure of pyrantrin (4-[(3-carboxy-2-hydroxynaphthalen-1-yl)methyl]-3-hydroxynaphthalene-2-carboxylic acid).

2. EXPERIMENTAL SECTION

2.1. Preparation of Inhibitor Stock Solution and Metal Dressing

5 g of the drug, obtained in a powdered form, was digested in a 1000 ml volumetric flask containing 1.0 M H₂SO₄ and allowed to completely dissolve for 48 hours. It was later filtered, and different inhibitor concentrations (500, 750, 1000, 125, and 1500 ppm) were prepared. The pieces of 1100-H14 aluminum alloy used for this work were obtained from Ibom Metal and Aluminum Company, Akwa Ibom State, Nigeria, with a composition of Cu (0.05 – 0.20 %), Fe (0.95 %), Mn (0.05 %), Si (0.95 %), Zn (0.1 %), Residuals (0.15 %) and Al (98.8 %) for aluminum. The metals were resized into 2.5 cm x 0.08 cm x 2.5 cm dimension for gravimetric analysis and 1 cm x 1 cm for electrochemical impedance analysis. All the resized metals were adequately polished with an electronic UNIPOL- 820 metallographic polishing machine to a mirror surface with different grades of emery papers (300, 1000, and 1200 grades), washed in distilled water, degreased in ethanol, rinsed in Acrastrip 600 Auto reagent, air dried and stored in a moisture free desiccator.

2.2. Mass Loss Experimentation

Polished coupons of dimension 2.5 cm x 0.08 cm x 2.5 cm were initially weighed, and readings were recorded. They were then immersed in the free solution of 1.0 M H₂SO₄ and other various inhibitor concentrations for 6 hours until the entire experimentation was completed. The coupons were removed from the solutions, washed with distilled water, rinsed in ethanol, degreased with Acrastrip 600 Auto reagent, air dried, and re-weighed every hour. The surface coverage and % inhibition efficiency of the inhibitor was determined from equation 1 and 2

$$\text{Surface coverage}(I) = \frac{(C_x - C_y)}{C_x} \quad (1)$$

$$\text{Inhibition efficiency}(\%F) = \frac{(C_x - C_y)}{C_x} \times 100 \quad (2)$$

where I is the surface coverage of the inhibitor, C_x and C_y are the corrosion rates of the free and inhibited solutions, and %F is the percentage inhibition efficiency of the inhibitor.

2.3. Electrochemical Method (EIS/PDP)

The EIS was conducted in a Gamry Reference 600 potentiostat. The reference electrode for the system was a saturated calomel (SCE) electrode, a 1 cm²

platinum foil was adopted as a counter electrode, and the working electrode was an aluminum coupon with dimensions 1 cm x 1 cm. Electrochemical tests were conducted within a frequency of 10 Hz - 100,000 Hz with an amplitude of 5 mV. The Potentiodynamic polarization measurement was carried out by altering the electrode potential from - 1.5 to + 1.5 V with respect to the open circuit potential (OCP) at a scan rate of 0.01 mV/s. All experiments were conducted every 60 min with the free and inhibited solutions. From b_{ct} and I_{corr} obtained, the surface coverage and inhibition efficiencies were calculated using Equation 3– 5, respectively.

$$I = \frac{b_{ct}^0 - b_{ct}^i}{b_{ct}^0} \quad (3)$$

$$\% \phi = \frac{b_{ct}^0 - b_{ct}^i}{b_{ct}^0} \times 100 \quad (4)$$

$$\% \phi = 100 \left[1 - \frac{I_{corr}^i}{I_{corr}^0} \right] \quad (5)$$

where I is the surface coverage of the inhibitor, b_{ct}⁰ and b_{ct}ⁱ represent the charge transfer resistance and I_{corr}⁰ and I_{corr}ⁱ is the corrosion density in the free and inhibited solutions of the inhibitor, respectively.

2.4. Computational Method

The studies were conducted with the Material Studio software (version 8.0). The quantum chemistry computations were performed using two computational programs, namely Vamp and Dmol3. Theoretical calculations were conducted at the Restricted Hartree-Fock level (RHF) utilizing the Hamiltonian parametric method 3 (PM3). Information obtained include higher occupied molecular orbital energy (E_{HOMO}), lower unoccupied molecular orbital energy (E_{LUMO}), Fukui positive and negative indices plots, HOMO and LUMO energy plots, energy gap (ΔE), chemical potential (μ), global hardness (η) and global softness (S), electrophilicity index (ω), according to equation 6 – 10 respectively.

$$\text{Energy gap}(\Delta E) = E_{HOMO} - E_{LUMO} \quad (6)$$

$$\text{Chemical potential}(\mu) = \frac{-(E_{HOMO} + E_{LUMO})}{2} \quad (7)$$

$$\text{Global hardness}(\eta) = \frac{(E_{HOMO} - E_{LUMO})}{2} \quad (8)$$

$$\text{Global softness}(S) = \frac{1}{2[(E_{HOMO} - E_{LUMO})]} \quad (9)$$

$$\text{Electrophilicity index}(\omega) = \frac{\mu^2}{2[(E_{HOMO} - E_{LUMO})]} \quad (10)$$

3. RESULTS AND DISCUSSION

3.1. Weight Loss

From Table 1, it was observed that the loosely bounded particles of the metal were affected by the acid attack, especially where no inhibitor was introduced. This could be due to dissolved non-volatile metal particles accumulating in solution over time (8, 10-13). However, it was not the case when the inhibitor was added, as the weight loss eventually began to decrease with time, implying that the

inhibitor prompted the reduction in the electron flow from the anode. This is again attributed to stronger phyto-atom adsorption on the surface, withholding

the dissociation process of loosely held particles (7, 11, 14).

Table 1: Weight loss data showing corrosion rate of 1100 – H14 aluminum, surface coverage, and inhibition efficiency of pyrantrin in 1m H₂SO₄ solutions.

Conc. (ppm)	Cor. Rate (mg/cm ² /hr)	Sur. Cov.	Inh. Eff. (%)
Blank	0.0042	-	-
500	0.0025	0.405	40.5
750	0.0019	0.548	54.8
1000	0.0016	0.619	61.9
1250	0.0008	0.810	81.0
1500	0.0002	0.952	95.2

3.2. Electrochemical Impedance Result

Data for the electrical interference of the system with the inhibitor are presented in Table 2, and the corresponding Nyquist plots are shown in Figures 2a-b. It was observed that the inhibitor showed a single capacity loop for 1100 - H14 Aluminum, which is directed toward a single charge transfer (6, 15-17). The sizes of these loops were observed to increase with the rise up to 2500 ppm, which is in line with the increased charge transfer values, indicating adsorption of the inhibitor on both surfaces and a reduction of the exposed area (active sites) of the metal (10,15,16). The data for the double-layer capacitance of the semicircle and inhibition efficiency were determined following Equation 11 - 12 and are presented in Tables 5 and 6.

$$C_{dl} = \frac{1}{\omega Z''} \tag{11}$$

where Z'' is the imaginary component of impedance at any frequency inside the semicircle and ω is the angular frequency (9,11).

$$\% \rho = \frac{b_{ct}^0 - b_{ct}^i}{b_{ct}^i} \times 100 \tag{12}$$

where b_{ct}⁰ and b_{ct}ⁱ correspond to the charge transfer values in the free and inhibited solutions of expired pyrantrin inhibitors, respectively.

Values from Table 2 showed increased charge transfer resistance as both metals were measured through increased concentration. Considering the increased values of the charge transfer resistance with inhibitor concentration, it is conclusive that a greater difficulty in charge transfer from metal to corrosive media was encountered in the presence of the pyrantrin inhibitor as the electrochemical process was affected; hence strong surface adsorption came to play as well as inhibition of corrosion active sites in metal (18-20).

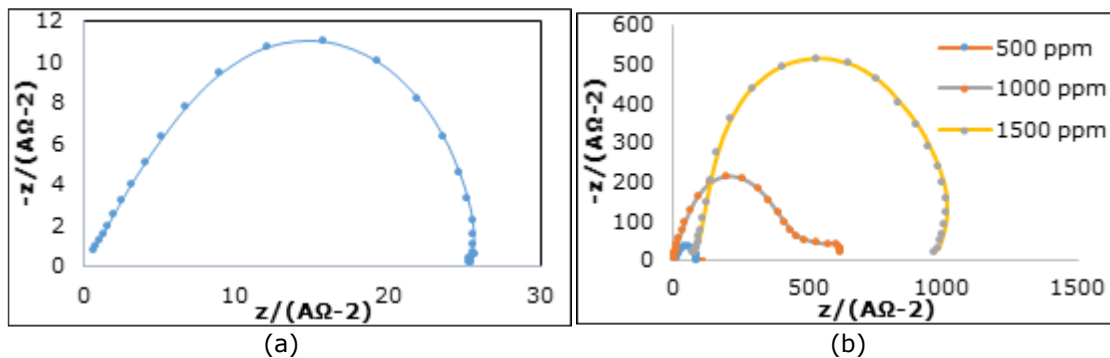


Figure 2: Nyquist plots for the corrosion inhibition of 1100–type aluminum (a) without and (b) with pyrantrin inhibitor in 1 M H₂SO₄ solutions.

Table 2: Nyquist plots values showing charge transfer resistance, double layer capacitance, and inhibition efficiency for the corrosion inhibition of 1100–type aluminum using pyrantrin inhibitor in 1 M H₂SO₄ solutions.

Conc. (ppm)	R _{ct} (A ⁻² Ω)	C _{dl}	IE (%)
Blank	26.4	6.658 x 10 ⁻⁶	-
500	97.6	4.586 x 10 ⁻⁶	72.9
1000	658	2.506 x 10 ⁻⁶	95.9
1500	889	2.267 x 10 ⁻⁶	97.0

In order to analyze the electrochemical system stability during the corrosion inhibition process with

and without the inhibitor, the Phase margins of the Bode plots were derived from the electrochemical

experiment, as shown in Fig. 3. From the plots (Figure 3), it was observed that all the phase lag data fitted well and gave rise to a positive phase margin and higher values (i.e., Blank – 120°, 500 ppm - 139°, 1000 ppm - 113° and 1500 ppm - 125°). This implies

that the inhibitor perfectly stabilized the system throughout the electrochemical process, which makes the pyrantrin inhibitor a good one for the corrosion inhibition of the metals (21-23).

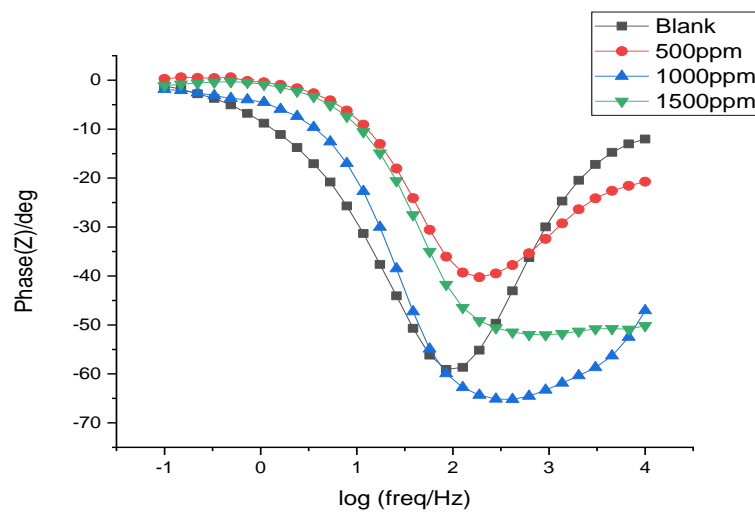


Figure 3: Bode plots for the corrosion inhibition of 1100 – H14 aluminum using pyrantrin inhibitor in 1 M H_2SO_4 solutions.

3.3. Potentiodynamic Polarization Result

Table 3 presents the potentiodynamic polarization values derived from the data depicted in Figure 4. The experimental results indicate that adding inhibitors caused a progressive shift in the corrosion potential values toward a more positive direction. This shift led to alterations in both the cathodic and anodic polarization branches. This observation suggests that the introduced inhibitor molecules mostly functioned as an anodic-type inhibitor (15, 19-21). This can also be confirmed by the anodic and cathodic Tafel slope values presented in Table 3. The

corrosion current density measurements exhibited a downward trend, whereas the comparable inhibition efficiency values derived from corrosion polarization demonstrated an upward trend for both metals when the inhibitor was present. This suggests that the extent of electron loss at the anode was negligible, hence indicating the absence of any oxidation reaction that could have led to the degradation (corrosion) of the anode. Therefore, it can be observed that the cathode remains unaltered (23-25).

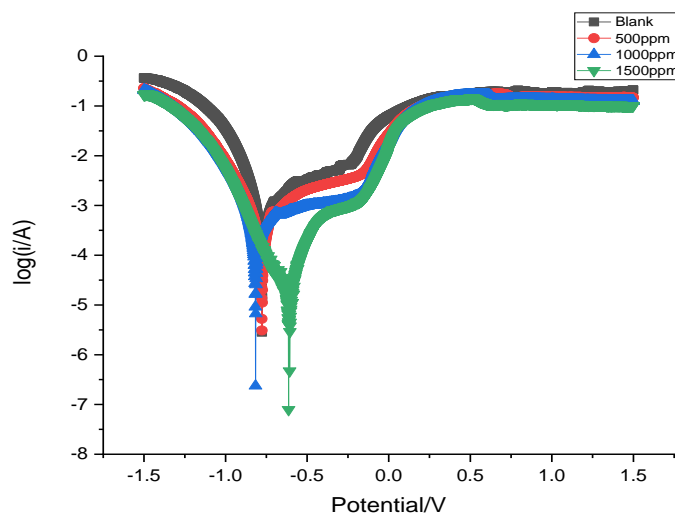


Figure 4: Tafel plots for the corrosion inhibition of 1100–type aluminum using pyrantrin inhibitor in 1 M H_2SO_4 solutions.

Table 3: Tafel plots values for the corrosion inhibition of 1100-type aluminum using pyrantrin inhibitor in 1 M H₂SO₄ solutions.

Conc. (ppm)	I _{corr} (μAcm ⁻²)	Slp _c (mV/dec)	Slp _a (mV/dec)	LP (Ω)	IE _{LP} (%)	IE _{Icorr} (%)	E _{corr} (mV)
Blank	9.905	9.706	8.211	1067	-	-	-9.368
500	4.231	7.969 [1.737]	4.179 [4.042]	116	89.1	57.3	-7.256
1000	3.366	7.765 [1.941]	2.661 [5.563]	106	90.1	66.0	-6.758
1500	3.138	4.763 [4.943]	1.412 [6.809]	53	95.0	68.3	-6.405

3.4. Quantum Chemical Calculations

After assessment of both the active component – pyrantel (C₁₁H₁₄N₂S) and the inactive components – Butylated hydroxytoluene (C₁₅H₂₄O), Citric acid monohydrate (C₆H₈O₇.H₂O), Potassium sorbate (C₆H₇O₂.K), Sodium benzoate (C₇H₅O₂.Na), Sucrose (C₁₂H₂₂O₁₁), Water (H₂O) and Xanthan gum of pyrantrin, the researcher concluded on applying the density functional theory (DFT) on the active component which is likely the effective contributor to the corrosion inhibition of 1100-H14 aluminum. This conclusion on the active component contribution to corrosion inhibition was drawn from the fact that the inactive component does not possess characteristics of a typical inhibitor, e.g., the presence of heteroatoms like N, S, P, etc., no double bond to access pi bonds, not aromatic, etc. Figures 5a -c show the optimized structure and the Frontier molecular orbitals (FMO) distribution density of the energy of

the highest occupied molecular orbital (EHOMO) and the energy of the lowest unoccupied molecular orbital (ELUMO) for pyrantel. It is evident from the figures that the electron density distribution at the highest occupied molecular orbital (HOMO) is localized strongly on the heteroatom (Nitrogen), carbon-carbon double bonds on the aromatic benzene ring and in methyl group (CH₃) present in pyrantel (Figures 5 d - e) (17-19). However, the electron density distribution for the lowest unoccupied molecular orbital (LUMO) was distributed on the individual carbon atoms on the aromatic ring and the Sulphur stereogenic centers (Figures 5 d - e). Therefore, the inhibitory power of pyrantrin can be explained mostly by the presence of π electrons and nitrogen heteroatoms favoring the sharing of electrons between the inhibitor and the metal surface (10-12, 23-26).

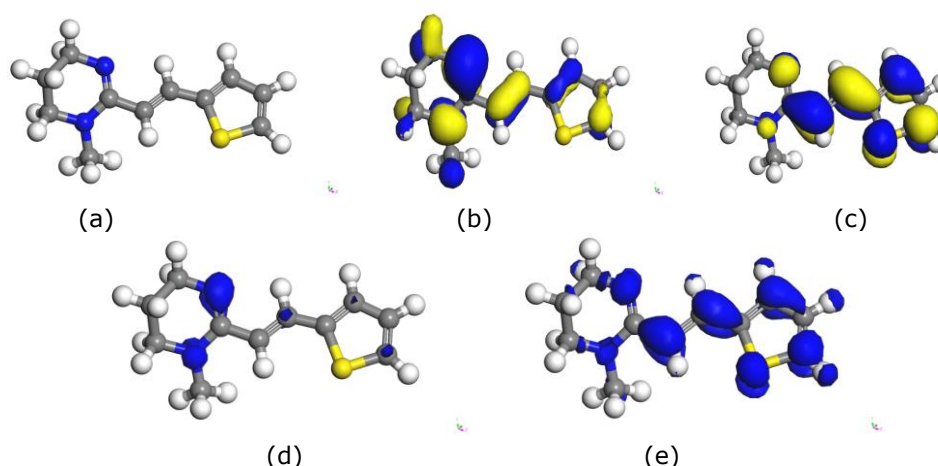


Figure 5: (a) Optimized structure, (b) Highest occupied molecular orbital and (c) Lowest unoccupied molecular orbital (d) Electrophilic (f-) and (e) Nucleophilic (f+) reactive sites of pyrantel molecule.

Table 4: Quantum chemical calculations values for pyrantel molecule.

Parameters	Data (eV)
E _{HOMO}	-4.075
E _{LUMO}	-2.154
ΔE (energy gap)	1.921
χ	3.114
η	0.961
σ	1.848
ω	5.045
δ	0.198
ΔN	2.969
ΔE _{b-d}	0.240
Binding energy	-132.9

Table 4 shows the quantum chemical parameters for pyrantel as an inhibitor of corrosion of 1100 – H14 aluminum. Absolute electronegativity (χ), global hardness (η), global softness (σ), electrophilicity index (ω), and nucleophilicity index (δ) were calculated from equation 13 – 17.

$$\chi = \frac{I.P.+E.A.}{2} \quad (13)$$

$$\eta = \frac{I.P.-E.A.}{2} \quad (14)$$

$$\sigma = \frac{1}{\eta} \quad (15)$$

$$\omega = \frac{\chi^2}{2\eta} \quad (16)$$

$$\delta = \frac{1}{\omega} \quad (17)$$

where ϕ_m is the work function for the metal surface (work function for Al (111) is 4.02eV), χ_i represents absolute electronegativity of the inhibitor, η_m , and η_i represents global hardness for the metal and inhibitor, respectively. The inhibitor was observed to have a lower energy gap (2.46 eV), suggesting a lower energy requirement for removing an electron from the highest occupied orbital, which entails a better inhibitor (16, 21, 26). From Table 4, the hardness's value was higher than that of softness. This implies a shorter energy gap between the inhibitor/metal interface and a possible lower dissociation energy, giving rise to stronger adsorption and better inhibition (22, 26-28). Also, the global electrophilicity index (ω) has a value of 5.045, implying a higher inhibition efficiency (28).

4. CONCLUSION

Arising from all the experimental techniques under study,

1. It is confirmed that pyrantrin was a reliable alternative inhibitor for inhibiting 1100 – H14 aluminum corrosion in a sulphuric acid environment.
2. Inhibition of corrosion on 1100 – H14 aluminum was observed through strong adsorption of pyrantrin molecules on the surface of the metals.
3. Electrochemical data was in good agreement with those of the chemical and theoretical as charge transfer resistance and inhibition efficiency were increasing while the double layer capacitance was decreasing with concentration, respectively. Features that are attributed to a good inhibitor.
4. Theoretical data shows that the inhibitor was good as the energy gap for pyrantrin was as low as 1.921 eV, and inhibition depends largely on the hetero-atoms of the major constituent of pyrantrin.

5. CONFLICT OF INTEREST

The authors declare no conflict of interest in the research work.

6. REFERENCES

1. Agwamba EC, Udoikono AD, Louis H, Udoh EU, Benjamin

I, Igbalagh AT, et al. Synthesis, characterization, DFT studies, and molecular modeling of azo dye derivatives as potential candidate for trypanosomiasis treatment. *Chem Phys Impact* [Internet]. 2022 Jun 1;4:100076. Available from: [<URL>](#).

2. Ameh PO, Eddy NO. Experimental and Computational Chemistry Studies on the Inhibition Efficiency of Phthalic Acid (PHA) for the Corrosion of Aluminum in Hydrochloric and Tetraoxosulphate (VI) Acids. *Prot Met Phys Chem Surfaces* [Internet]. 2018 Nov 28;54(6):1169–81. Available from: [<URL>](#).

3. Ammouchi N, Allal H, Belhocine Y, Bettaz S, Zouaoui E. DFT computations and molecular dynamics investigations on conformers of some pyrazinamide derivatives as corrosion inhibitors for aluminum. *J Mol Liq* [Internet]. 2020 Feb 15;300:112309. Available from: [<URL>](#).

4. Bashir S, Sharma V, Kumar S, Ghelichkhah Z, Obot IB, Kumar A. Inhibition Performances of Nicotinamide Against Aluminum Corrosion in an Acidic Medium. *Port Electrochim Acta* [Internet]. 2020;38(2):107–23. Available from: [<URL>](#).

5. Ugi BU. Corrosion Inhibition of Cu-Zn-Fe Alloy in Hydrochloric Acid Medium by Crude Ethanol Extracts from Roots-Leaves Synergy of Solanum melongena. *Earthline J Chem Sci* [Internet]. 2020 Nov 27;5(1):105–18. Available from: [<URL>](#).

6. Buvaneswari M, Santhakumari R, Usha C, Jayasree R, Sagadevan S. Synthesis, growth, structural, spectroscopic, optical, thermal, DFT, HOMO–LUMO, MEP, NBO analysis and thermodynamic properties of vanillin isonicotinic hydrazide single crystal. *J Mol Struct* [Internet]. 2021 Nov 5;1243:130856. Available from: [<URL>](#).

7. Diki NYS, Coulibaly NH, Kambiré O, Trokourey A. Experimental and Theoretical Investigations on Copper Corrosion Inhibition by Cefixime Drug in 1M HNO₃ Solution. *J Mater Sci Chem Eng* [Internet]. 2021 May 21;9(5):11–28. Available from: [<URL>](#).

8. Ebenso EE, Verma C, Olasunkanmi LO, Akpan ED, Verma DK, Lgaz H, et al. Molecular modelling of compounds used for corrosion inhibition studies: a review. *Phys Chem Chem Phys* [Internet]. 2021 Sep 22;23(36):19987–20027. Available from: [<URL>](#).

9. Erteeb MA, Ali-Shattle EE, Khalil SM, Berbash HA, Elshawi ZE. Computational Studies (DFT) and PM3 Theories on Thiophene Oligomers as Corrosion Inhibitors for Iron. *Am J Chem* [Internet]. 2021;11(1):1–7. Available from: [<URL>](#).

10. Ugi BU, Obeten ME, Bassey VM, Boekom EJ, Omaliko EC, Ugi FB, et al. Quantum and Electrochemical Studies of Corrosion Inhibition Impact on Industrial Structural Steel (E410) by Expired Amiloride Drug in 0.5 M Solutions of HCl, H₂SO₄ and NaHCO₃. *Moroccan J Chem* [Internet]. 2021 Dec 4;9(4):677–96. Available from: [<URL>](#).

11. Fouda AE-AS, El-Askalany AH, Molouk AFS, Elsheikh NS, Abousalem AS. Experimental and computational chemical studies on the corrosion inhibitive properties of carbonitrile compounds for carbon steel in aqueous solutions. *Sci Rep* [Internet]. 2021 Nov 4;11(1):21672. Available from: [<URL>](#).

12. Joshi BD, Thakur G, Chaudhary MK. Molecular Structure, Homo-Lumo and Vibrational Analysis Of Ergoline By Density Functional Theory. *Sci World* [Internet]. 2021 Feb 15;14(14):21–30. Available from: [<URL>](#).

13. Liu Q, Song Z, Han H, Donkor S, Jiang L, Wang W, et al. A novel green reinforcement corrosion inhibitor

extracted from waste *Platanus acerifolia* leaves. *Constr Build Mater* [Internet]. 2020 Nov 10;260:119695. Available from: [<URL>](#).

14. Majd MT, Ramezanzadeh M, Ramezanzadeh B, Bahlakeh G. Production of an environmentally stable anti-corrosion film based on Esfand seed extract molecules-metal cations: Integrated experimental and computer modeling approaches. *J Hazard Mater* [Internet]. 2020 Jan 15;382:121029. Available from: [<URL>](#).

15. Onyeachu IB, Abdel-Azeim S, Chauhan DS, Quraishi MA. Electrochemical and Computational Insights on the Application of Expired Metformin Drug as a Novel Inhibitor for the Sweet Corrosion of C1018 Steel. *ACS Omega* [Internet]. 2021 Jan 12;6(1):65-76. Available from: [<URL>](#).

16. Uwah IE, Ugi BU, Okafor PC, Ikeuba AI. Investigation of the corrosion inhibition effects of Bitters on Mild Steel in acidic medium: A case study of *Andrographis paniculata* and *Vernonia amygdalina*. In: *Proceedings of the 35th Annual International Conference, Workshop and Exhibition of the Chemical Society of Nigeria (CSN)*. 2012. p. 304-9.

17. Padash R, Sajadi GS, Jafari AH, Jamalizadeh E, Rad AS. Corrosion control of aluminum in the solutions of NaCl, HCl and NaOH using 2,6-dimethylpyridine inhibitor: Experimental and DFT insights. *Mater Chem Phys* [Internet]. 2020 Apr 1;244:122681. Available from: [<URL>](#).

18. Rbaa M, Ouakki M, Galai M, Berisha A, Lakhrissi B, Jama C, et al. Simple preparation and characterization of novel 8-Hydroxyquinoline derivatives as effective acid corrosion inhibitor for mild steel: Experimental and theoretical studies. *Colloids Surfaces A Physicochem Eng Asp* [Internet]. 2020 Oct 5;602:125094. Available from: [<URL>](#).

19. Sharma S, Ganjoo R, Kr. Saha S, Kang N, Thakur A, Assad H, et al. Experimental and theoretical analysis of baclofen as a potential corrosion inhibitor for mild steel surface in HCl medium. *J Adhes Sci Technol* [Internet]. 2022 Oct 2;36(19):2067-92. Available from: [<URL>](#).

20. Ugi BU, Obeten ME, Bassey VM, Hitler L, Adalikwu SA, Omaliko CE, et al. Adsorption and Inhibition Analysis of Aconitine and Tubocurarine Alkaloids as Eco-friendly Inhibitors of Pitting Corrosion in ASTM – A47 Low Carbon Steel in HCl Acid Environment. *Indones J Chem* [Internet]. 2022 Jan 25;22(1):1-16. Available from: [<URL>](#).

21. Solomon MM, Umoren SA, Quraishi MA, Tripathy DB, Abai EJ. Effect of alkyl chain length, flow, and temperature on the corrosion inhibition of carbon steel in a simulated acidizing environment by an imidazoline-based inhibitor. *J Pet Sci Eng* [Internet]. 2020 Apr 1;187:106801. Available from: [<URL>](#).

22. Su P, Li L, Li W, Huang C, Wang X, Liu H, et al. Expired Drug Theophylline as Potential Corrosion Inhibitor for 7075 Aluminium Alloy in 1M NaOH Solution. *Int J Electrochem Sci* [Internet]. 2020 Feb 1;15(2):1412-25. Available from: [<URL>](#).

23. Tan J, Guo L, Wu D, Wang S, Yu R, Zhang F, et al. Electrochemical and Computational Studies on the Corrosion Inhibition of Mild Steel by 1-Hexadecyl-3-methylimidazolium Bromide in HCl Medium. *Int J Electrochem Sci* [Internet]. 2020 Mar 1;15(3):1893-903. Available from: [<URL>](#).

24. Zaher A, Chaouiki A, Salghi R, Boukhraz A, Bourkhiss B, Ouhssine M. Inhibition of Mild Steel Corrosion in 1M Hydrochloric Medium by the Methanolic Extract of *Ammi visnaga* L. Lam Seeds. *Int J Corros* [Internet]. 2020 Jan 5;2020:9764206. Available from: [<URL>](#).

